Acoustic Signature from Flames as a Combustion Diagnostic Tool

M. K. Ramachandra* and W. C. Strahle†
Georgia Institute of Technology, Atlanta, Georgia

A nonintrusive acoustic technique has been developed to obtain the fluctuating heat release rate distribution in open premixed turbulent flames. Propane-air flames of equivalence ratio 0.6, 0.8, and 1.0 with a 16.4 mm diam burner and a 11.55 m/s mean flow speed have been employed. The flame sound pressures in the near field were measured in an anechoic chamber. With the acoustic spectra as the input, the heat release rate spectral information was obtained by numerically using an augmented Galerkin method to solve a Fredholm integral equation of the first kind. Computed results have been qualitatively verified by C_2 emission studies. The experimentally observed correspondence between mean and rms C_2 emission intensity implies that the shape of the mean heat release rate distribution can, in principle, be deduced by the acoustic technique.

Nomenclature

A = area of flame cross section
a = coefficients in Galerkin expansion
D = burner diameter
E = light emission function
F = defined in Eq. (5)
f = frequency, Hz, unknown function in Eq. (8)
G = free-space Green's function
g = known function in Eq. (8)
H = heat release fluctuation function
I = emission intensity
i = $\sqrt{-1}$, index
K = kernel of Eq. (8)
k = wave number
L = flame length
$L_{\hat{Q}}$ = length scale
N = number of terms in Galerkin expansion
p = acoustic pressure
Q = heat release rate per unit volume
r = constraint parameter
S_{RR} = autospectral density of sound at location x_R
S_{12} = cross-spectral density of light emissions from flame cross sections at x_1 and x_2
T = sample time for finite Fourier transform
t = time
U = flow speed
u_ω = defined in Eq. (1)
V = reaction volume
x = coordinate vector (x,y,z)
Z = defined in Eq. (3)
γ = ratio of specific heats
λ = constraint parameter
ξ = separation distance between flame cross sections at x_1 and x_2
ϕ = equivalence ratio
ω = circular frequency, rad/s

Superscripts

T = transpose of a matrix
$\bar{(\ )}$ = ensemble average
$(\ )^*$ = complex conjugate
$\tilde{(\ )}$ = approximate value
$\hat{(\ )}$ = cross-sectional quantity

Subscript

ω = finite Fourier transform

Presented as Paper 82-0039 at the AIAA 20th Aerospace Sciences Meeting, Orlando, Fla., Jan. 11-14, 1982; submitted Jan. 20, 1982; revision received Nov. 29, 1982.

*Post Doctoral Fellow, School of Aerospace Engineering. Currently, Post Doctoral Fellow, Dept. of Chemical Engineering, Louisiana State University, Baton Rouge, La. Member AIAA.

†Regents' Professor, School of Aerospace Engineering. Associate Fellow AIAA.

I. Introduction

A NONINTRUSIVE technique to determine the heat release rate distribution and its turbulence properties would be a useful tool in combustor development. The heat release rate distribution is intimately linked to questions of flame stability, liner life, pollutant formation, and combustion efficiency. This paper deals with the development of a nonintrusive method for measuring heat release rate fluctuations by an acoustic method. The relation of the fluctuating field to the mean field is also investigated. As a first step, the experimental configuration is a simple one—that of an open premixed turbulent flame.

Utilized as the diagnostic method is the combustion noise output from a turbulent flame. Under appropriate restrictions, this noise output can be theoretically linked to the fluctuating heat release rate. As a verification of the results obtained by the acoustic method, emissions from C_2 radicals are also measured and linked with the heat release rates.

II. Theory

The starting point is an approximate combustion noise equation derived by Strahle[1-3] following a Lighthill-type acoustic analogy approach,

$$\nabla^2 p_\omega(x) + k^2 p_\omega(x) = -u_\omega(x) \tag{1}$$

where $u_\omega = (\gamma - 1)i\omega Q_\omega$. This is an inhomogeneous Helmholtz equation for the acoustic pressure from a turbulent flame, the source function being the fluctuating heat release. $u_\omega(x)$ is nonzero only when x is inside the reacting volume (Fig. 1). The subscript ω denotes a finite Fourier transform, that is,

$$p_\omega(x) = \int_0^T p(x,t)\, e^{-i\omega t}\, dt$$

where T is a finite sample time that is large compared to the minimum period to be resolved.

The solution[4] to Eq. (1) subject to Sommerfeld's radiation condition is

$$p_\omega(x) = \int_V u_\omega(x_0)\, G(x,x_0)\, dV_0$$

where G is the free-space Green's function defined by

$$G(x,x_0) = \frac{\exp(-ik\,|x-x_0|)}{4\pi\,|x-x_0|}$$

For combustion noise, p_ω is a random function of frequency. It is convenient to work with spectral densities that yield stable values of the frequency content of the signals.[5] It is assumed that the random process is weakly stationary. The autospectral density is given by

$$S_{RR} \equiv \overline{p_\omega^*(x_R)\,p_\omega(x_R)}/T$$

It is always a real-valued non-negative function and gives the frequency distribution of the mean square fluctuation. The total area under a plot of the autospectral density vs frequency gives the mean square value of the random signal. The bar superscript indicates an average of the conjugate product taken over several sample records of length T.

Substituting for p_ω,

$$S_{RR} = \frac{1}{T}\overline{\left[\int_{V_1} u_\omega^*(x_1)\,G^*(x_R,x_1)\,\mathrm{d}V_1\right]} \times \overline{\left[\int_{V_2} u_\omega(x_2)\,G(x_R,x_2)\,\mathrm{d}V_2\right]}$$

or

$$S_{RR} = \int_{V_2}\int_{V_1} G^*(x_R,x_1)\,G(x_R,x_2)\left[\overline{\frac{u_\omega^*(x_1)\,u_\omega(x_2)}{T}}\right]\mathrm{d}V_1\,\mathrm{d}V_2$$

This is a six-dimensional integral equation of the first kind for the term in the square brackets, which is the cross-spectral density of the heat release rate fluctuations at locations x_1 and x_2 in the reacting volume $V_1 \equiv V \equiv V_2$. S_{RR} can be measured. The problem, then, is to solve the above equation. It is known[6,7] that equations of this type are difficult to solve. Here, the task is formidable because S_{RR} is a measured quantity that will contain error. Some simplification is needed to expedite the solution process. It is experimentally observed that, for the flames employed in this program, the flame length is an order of magnitude longer than the burner diameter. It is, therefore, reasonable to assume that the flame is effectively a line source along the x axis. Further confining the measurement of S_{RR} to the horizontal plane through the burner ($z_R = 0$), one has the approximation

$$|x_R - x_1| \cong [(x_R - x_1)^2 + y_R^2]^{1/2}$$

Then

$$S_{RR} = \int_0^L\int_0^L \mathrm{d}x_1\,\mathrm{d}x_2\,\frac{\exp[ik\sqrt{(x_R-x_1)^2+y_R^2}]}{4\pi\sqrt{(x_R-x_1)^2+y_R^2}} \times \frac{\exp[-ik\sqrt{(x_R-x_2)^2+y_R^2}]}{4\pi\sqrt{(x_R-x_2)^2+y_R^2}}\,Z(x_1,x_2) \qquad (2)$$

where

$$Z(x_1,x_2) = \int_{A_1}\mathrm{d}A_1\int_{A_2}\mathrm{d}A_2\,\overline{\frac{u_\omega^*(x_1)\,u_\omega(x_2)}{T}} \qquad (3)$$

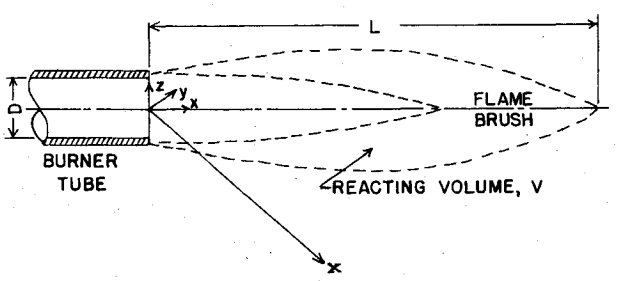

Fig. 1 Coordinate system.

where Z is proportional to the cross-spectral density of the heat release rate fluctuations at flame cross sections located at x_1 and x_2. Let

$$x_2 = x_1 + \xi$$

where ξ is the separation distance along the burner axis between points x_1 and x_2. As the separation distance increases, the heat release rate fluctuations become less correlated and the magnitude of Z approaches zero. Results from optical experiments, reported below, indicate this trend. In fact, Z drops to zero fast enough so that one can write

$$\int_0^L \mathrm{d}x_1\int_0^L \mathrm{d}x_2 Z(x_1,x_2) \cong \int_0^L \mathrm{d}x_1\int_{-\infty}^{\infty}\mathrm{d}\xi\,Z(x_1,\xi)$$

The autospectral density becomes

$$S_{RR} = \int_0^L \mathrm{d}x_1\int_{-\infty}^{\infty}\mathrm{d}\xi\,\frac{\exp[ik\sqrt{(x_R-x_1)^2+y_R^2}]}{4\pi\sqrt{(x_R-x_1)^2+y_R^2}} \times \frac{\exp[-ik\sqrt{(x_R-x_1-\xi)^2+y_R^2}]}{4\pi\sqrt{(x_R-x_1-\xi)^2+y_R^2}}\,Z(x_1,\xi) \qquad (4)$$

Equations (2) and (4) are two-dimensional integral equations for Z.

If it can be assumed that the length scale for the heat release rate fluctuations can be neglected compared to the flame length (see Sec. V, Fig. 7), further simplification is possible. Equation (4) reduces to

$$S_{RR} = \frac{1}{16\pi^2}\int_0^L \frac{\mathrm{d}x_1}{(x_R-x_1)^2+y_R^2}\int_{-\infty}^{\infty}\mathrm{d}\xi\,Z(x_1,\xi)$$

By definition of Z,

$$Z(x_1,\xi) \propto \overline{\hat{Q}_\omega^*(x_1)\,\hat{Q}_\omega(x_2)}$$

The superscript ($\hat{}$) indicates a cross-sectional quantity. Here $\hat{Q}_\omega(x_2)$ can be expected to behave like $\hat{Q}_\omega(x_1)$ convected downstream at a characteristic speed U and subject to a decay that is some function of ξ. That is, as an approximate expectation

$$\hat{Q}_\omega(x_2) \cong \hat{Q}_\omega(x_1)\exp\left(-\frac{i\omega}{U}\xi\right)\psi(\xi)$$

Optical emission studies (see Sec. V) support this reasoning; $\psi(\xi)$ appears to be an exponentially decaying function. Therefore,

$$Z(x_1,\xi) \propto \overline{\hat{Q}_\omega^*(x_1)\,\hat{Q}_\omega(x_1)}\exp\left(-\frac{i\omega}{U}\xi\right)\psi(\xi)$$

$$\int_{-\infty}^{\infty} Z(x_1,\xi)\,\mathrm{d}\xi \propto \overline{\hat{Q}_\omega^*(x_1)\,\hat{Q}_\omega(x_1)}\int_{-\infty}^{\infty}\exp\left(-i\frac{\omega}{U}\xi\right)\psi(\xi)\,\mathrm{d}\xi$$

$$= \overline{\hat{Q}_\omega^*(x_1)\,\hat{Q}_\omega(x_1)}\int_{-\infty}^{\infty}\cos\left(\frac{\omega}{U}\xi\right)\psi(\xi)\,\mathrm{d}\xi$$

= [autospectral density of $\hat{Q}_\omega(x_1)$] [length scale]

Then, say

$$\int_{-\infty}^{\infty} Z(x_1,\xi)\,\mathrm{d}\xi = Z(x_1,0)\,L_{\hat{Q}} = F(x_1) \qquad (5)$$

$L_{\hat{Q}}$ is a length scale defined as

$$L_{\hat{Q}} = \int_{-\infty}^{\infty}\mathrm{Re}[Z(x_1,\xi)]\mathrm{d}\xi/Z(x_1,0) \qquad (6)$$

Finally,

$$S_{RR} = \frac{1}{16\pi^2} \int_0^L \frac{F(x)\,dx}{(x_R - x)^2 + y_R^2} \tag{7}$$

As a result of the last simplification, Eq. (4) has been reduced to a one-dimensional problem [Eq. (7)]. Since $u_\omega \propto \omega Q_\omega$,

$$F(x) \propto \omega^2 S_{\hat{Q}\hat{Q}} L_{\hat{Q}}$$

At a given frequency, $F(x)$ is proportional to the product of the autospectral density and length scale of the heat release rate fluctuations at a flame cross section located at a distance x from the burner port. If y_R is considered fixed, then the inversion process requires the combustion noise autospectral density S_{RR} as a function of x_R over the interval $[0,L]$.

The integral equation approach is necessary to avoid intrusive measurements in the flame. The integral equations still require measurements close to the flame because, in the far field, the Green's functions can be brought out of the integral sign—which defeats the method. Therefore, near-field measurements are essential.

III. Method of Solution

The general form of a first-kind Fredholm equation is

$$\int_a^b K(x,y) f(y)\,dy = g(x), \quad a \le x \le b \tag{8}$$

where $K(x,y)$ and $g(x)$ are known functions and $f(x)$ is the unknown. K is called the kernel of the equation. Equations of this type are in general ill-posed; small errors in $g(x)$ can cause large "unphysical" oscillations in the solution predicted by the integral equation. Special techniques are available to control the instability. Various methods were investigated and the augmented Galerkin technique[8] was chosen. Essentially, the Galerkin matrices are augmented by a set of constraints on the unknown coefficients and the augmented equations are solved as a problem in linear programming. Let

$$\tilde{f}(x) = \sum_{i=1}^{N} a_i \phi_i(x) \tag{9}$$

where $\{\phi_i\}$ is a complete set of functions orthogonal on $[a,b]$. The Galerkin equations for the coefficients are

$$\boldsymbol{B}\boldsymbol{a} = \boldsymbol{g} \tag{10}$$

Here

$$B_{ij} = \int_a^b \phi_i(x)\,dx \int_a^b K(x,y)\,\phi_j(y)\,dy, \quad i,j = 1,2,\ldots,N$$

$$g_i = \int_a^b g(x)\,\phi_i(x)\,dx, \quad i = 1,2,\ldots,N$$

$$\boldsymbol{a} = [a_1, a_2, \ldots, a_N]^T$$

As mentioned earlier, an attempt to solve Eq. (10) directly gives rise to wild oscillations in $\tilde{f}$ for large N. If Eq. (8) indeed has a solution, since $\{\phi_i(x)\}$ is a complete set, the series of Eq. (9) must be convergent as $N \to \infty$. That is,

$$\sum_{i=1}^{\infty} a_i^2 < \infty$$

Hence, there exist positive constants C_f and r such that

$$|a_i| \le C_f / (\hat{i})^r = \delta_i, \quad i = 1,2,\ldots,N$$

where

$$\hat{i} = 1, \quad i = 1$$

$$= i - 1, \quad i > 1$$

Given an estimate of C_f and r, the augmented Galerkin method requires one to solve the problem

$$\text{minimize } \|\boldsymbol{B}\boldsymbol{a} - \boldsymbol{g}\| \tag{11}$$

subject to

$$|a_i| \le \delta_i, \quad i = 1,2,\ldots,N$$

For numerical convenience in linear programming, Eq. (11) can be written in the form

$$\text{minimize } S = \sum_{i=1}^{N} \left| \sum_{j=1}^{N} B_{ij} a_j - g_i \right| \tag{12}$$

subject to

$$|a_i| \le \delta_i$$

The constrained optimization problem of Eq. (12) is then transformed into a problem in linear programming, which is basically a systematic method for minimizing (or maximizing) a function of several variables subject to constraints in the form of equations and inequalities. Both the function to be optimized and the constraints must be linear. Standard computer programs are available to solve linear programming problems when the number of variables and constraints becomes large.

It is claimed that the method is stable as the number of terms in the expansion increases and that the results are insensitive to the values of C_f and r. Recommended values for the two parameters are:

1) $r = 2, 3$.

2) $C_f = \lambda \|\boldsymbol{g}\| / \|\boldsymbol{B}\|$ where $\lambda = 2\text{-}4$.

The method was applied to Eq. (7) for a test case. Stable results were obtained even with perturbed data. Also the solutions converged quickly and turned out to be not influenced by the choice of constraints (variation in λ and r). Complete details are given in Ref. 9.

IV. Experimental Procedures

Three types of experiments were conducted:

1) Acoustic experiments in which sound pressures in the near field are measured.

2) Optical experiments in which cross-spectral densities of the emission intensity of C_2 radicals from different cross sections of the flames are determined.

3) Correlation experiments in which the optical and acoustic emissions are correlated.

The optical experiments obtain the heat release rate spectral densities directly to within a factor of a constant. These were used to qualitatively check the results from the acoustic technique.

All of the experiments were carried out inside an anechoic chamber. The chamber ($4 \times 3 \times 2$ m) has fiberglass inner walls that are efficient in absorbing the incident sound waves. Thus, acoustic measurements can be made in conditions close to those in a free field. The chamber also serves the secondary purpose of preventing drafts around the flame.

The burner is made of coaxial tubes. The mixture of propane and air flows through the inner tube. Hydrogen for the stabilizing diffusion flame is supplied through the annular space between the tubes. The inner tube has an inside diameter of 16.4 mm. A straight length of 50 diameters is provided to insure fully developed turbulent flow at the burner exit. A

mixing chamber filled with 4 mm glass balls is introduced in the main burner tube just before the 50 diam straight length. The chamber also serves as a flashback suppressor. The burner is mounted in the anechoic chamber with its axis horizontal. Reference 10 has more information on the flow system.

Spectral analysis of the recorded signals was done by a Hewlett Packard 5451A Fourier analyzer. This machine converts the data to digital form and computes the spectra using a fast Fourier transform algorithm.

Acoustic Experiments

The integral equations formulated earlier call for combustion noise data in the near field. It was also stipulated that the measurements be made in the horizontal plane through the burner axis.

Sound pressures are measured by Brüel and Kjaer 12.7 mm condenser microphones. Four such microphones are mounted on a stand at the same height as and along a line parallel to the burner. They are suitably spaced (100 mm apart) so as to cover the length of the flame. The microphones are traversed in steps of 25 mm in directions both parallel and perpendicular to the flame axis, thus obtaining data in a two-dimensional grid.

A far-field ($x_R = 0$, $y_R = 2.4$ m) measurement is taken with a single microphone. This is required for acoustic power calculations as explained later.

Optical Experiments

These experiments are planned to provide independent experimental support for the acoustic method. There is evidence[10-12] that the heat release rate fluctuations in a turbulent flame which generate sound also cause fluctuations in the emission intensity of C_2 and CH radicals. These are known to exist only in the reaction zone of hydrocarbon + air flames. Hurle et al.[11] found that the emission intensity is directly proportional to the rate of combustion.

The acoustic technique is designed to give the spectral density of the heat release rate fluctuations from the cross sections of the flame. Accordingly, the light experiments are tailored to obtain the emission intensity of C_2 radicals from different flame cross sections. Light signals from any two cross sections have to be recorded simultaneously to obtain the cross-spectral density.

The anechoic chamber served as a dark chamber for these experiments. A schematic is shown in Fig. 2. A 2:1 image of the flame is formed by a large lens. At the image plane of the burner axis, there are two vertical slits. These are quite narrow, 0.8 mm wide. Each slit receives light from a particular cross section of the flame. One of the slits is fixed in position, while the other can be moved parallel to the flame. A front surface mirror is mounted directly behind and attached to the movable slit. When this slit is moved, the mirror moves with it, always reflecting the light from the slit toward the same phototube. Associated with each slit is a narrow-band optical filter centered on a radiation band of C_2 radicals[11] (5165 Å). The filters have a peak transmission at 5145 Å with a half-peak transmittance bandwidth of 80 Å. The photomultiplier tubes are of EMI types 9637B and 9656B. The current signal from each phototube is passed through a 10 KΩ resistance to convert it into a voltage signal, which is then amplified and recorded.

Correlation Experiments

The objective here is to verify the correspondence between overall light and acoustic emissions for the present setup. For this purpose, an image of the entire flame is focused on a phototube after passing the light through a C_2 filter. The output of the phototube is proportional to the C_2 emission intensity integrated over the entire reacting volume. A microphone is placed in the far field. The signals from the phototube and the microphone are suitably amplified and recorded.

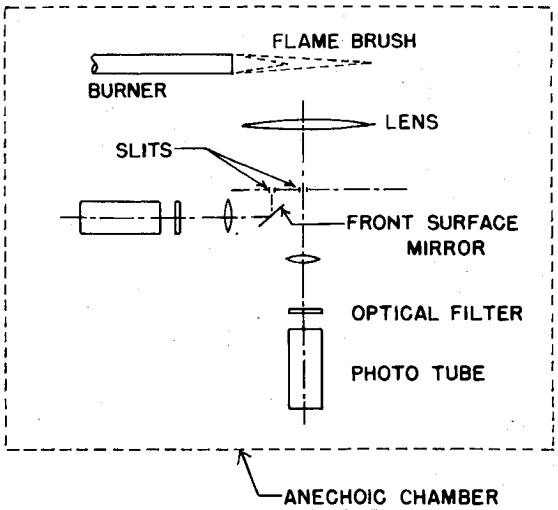

Fig. 2 Data acquisition schematic for optical experiments.

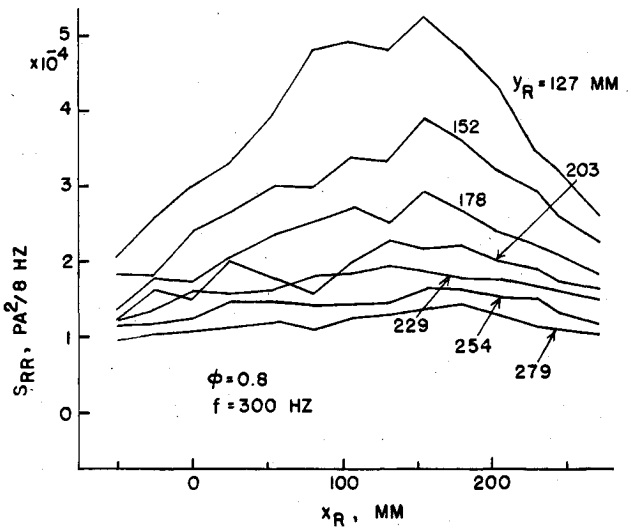

Fig. 3 Combustion noise autospectral density in near field.

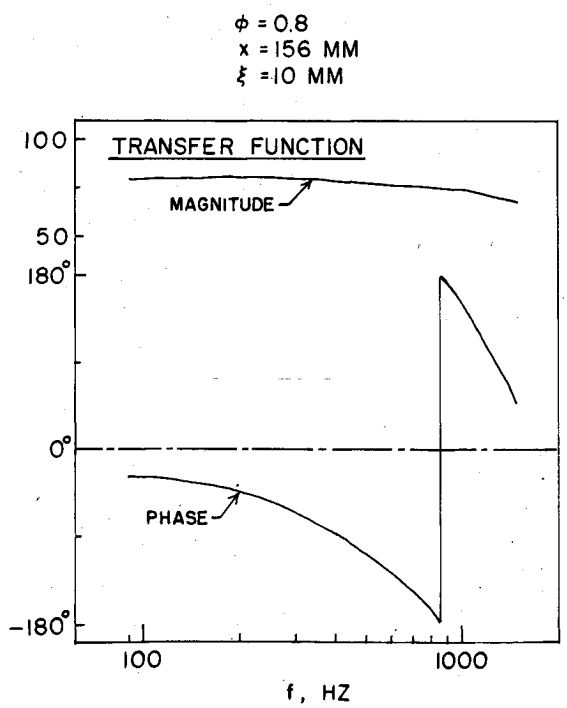

Fig. 4 Transfer function of two space-separated light signals.

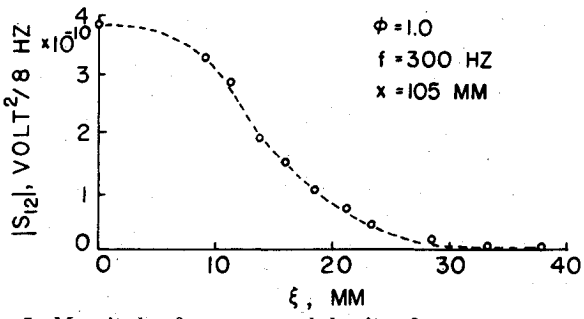

Fig. 5 Magnitude of cross-spectral density of two space-separated light signals as a function of the separation distance.

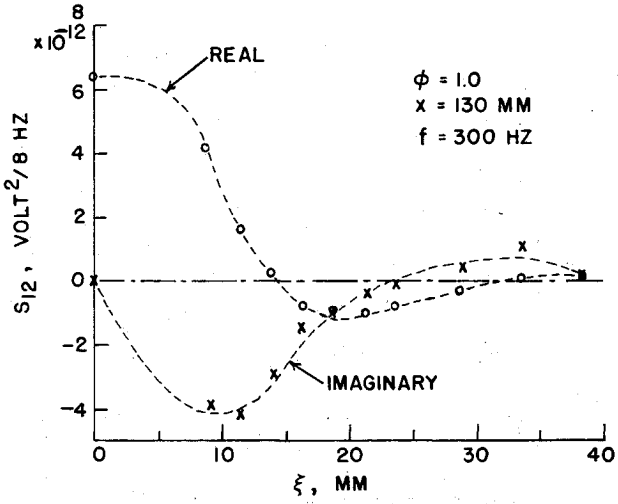

Fig. 6 Cross-spectral density of two space-separated light signals as a function of the separation distance.

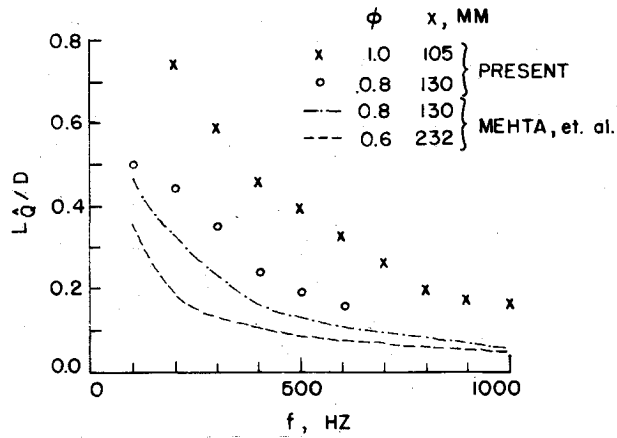

Fig. 7 Integral length scale variation with frequency.

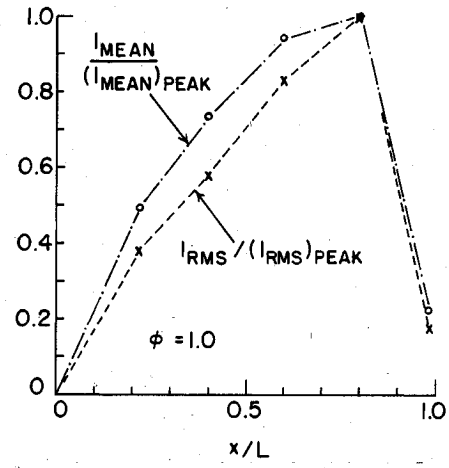

Fig. 8 Mean and rms light emission intensity vs length along flame axis.

V. Experimental Results

Acoustic Experiments

Sound pressures were measured in the near field for flames of equivalence ratios 0.6, 0.8, and 1.0 at a flow speed of 11.55 m/s. In all cases, the combustion noise was significantly greater than the noise due to the air jet alone. Typical autospectra are displayed in Fig. 3. These were obtained by Fourier analysis of the pressure signals with a 50 sample averaging and a further frequency smoothing over a 104 Hz bandwidth.

Optical Experiments

Figure 4 shows the transfer function of C_2 emission intensity for $\phi = 0.8$; the two cross sections of the flame are separated by 10 mm. The fixed slit is at $x = 156$ mm. This lies in the turbulent brush region of the flame. The phase of the transfer function is seen to drop linearly with frequency. This is due to convection caused by the mean flow of the reactants. The mean flow velocity calculated from the slope of the plot gave a value close to the mass weighted mean velocity.

Cross-spectral density plots are given in Figs. 5 and 6. They suggest a relation of the form

$$S_{12} = S_{11}\exp\left(-i\frac{\omega}{U}\xi\right)\psi(\xi)$$

Here $\exp[-i(\omega/U)\xi]$ is the convection factor and ψ a decaying function of ξ.

S_{12} corresponds to the quantity $Z(x_1,x_2)$ defined earlier where Z is related to the sound spectral density through an integral equation. The corresponding length scale here is given by

$$L_{\hat{Q}} = \frac{1}{S_{11}}\int_{-\infty}^{\infty}\mathrm{Re}[S_{12}]d\xi = \frac{2}{S_{11}}\int_{0}^{\infty}\mathrm{Re}[S_{12}]d\xi \qquad (13)$$

by symmetry.

Calculations show that a good approximation to the integral in Eq. (13) is obtained by considering the area under the $\mathrm{Re}[S_{12}]$ vs ξ curve up to the first minimum. Calculated length scales are given in Fig. 7 for two cases. They exhibit a rapid fall off with frequency.

In hydrocarbon flames there is intense ionization in the reaction zone. Wortberg[13] observed a nearly one-to-one correspondence between local heat release rate and ion concentration in laminar flames. Mehta et al.[14] have shown that ionization probes can be used to deduce local heat release rate in turbulent flames. Using a point ionization probe they obtained length scales [defined by Eq. (13)] in open premixed propane-air flames. These are reproduced in Fig. 7. For the case $\phi = 0.8$, $x = 130$ mm, for which the ionization results are available, there is good agreement between the optical and ionization results.

Correspondence between Fluctuating and Mean Heat Release Rate

The mean heat release rate distribution in a flame is of practical importance. The acoustic technique cannot give the mean heat release rate since the microphones sense only pressure fluctuations. The optical method has no such restriction. Figure 8 is a plot of the mean and the rms values of the C_2 emission intensity along the flame axis. It is interesting to note that both the curves have essentially the same

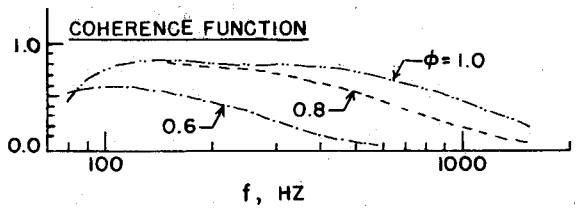

Fig. 9 Coherence between far-field sound pressure and time derivative of overall light emission intensity for various flames.

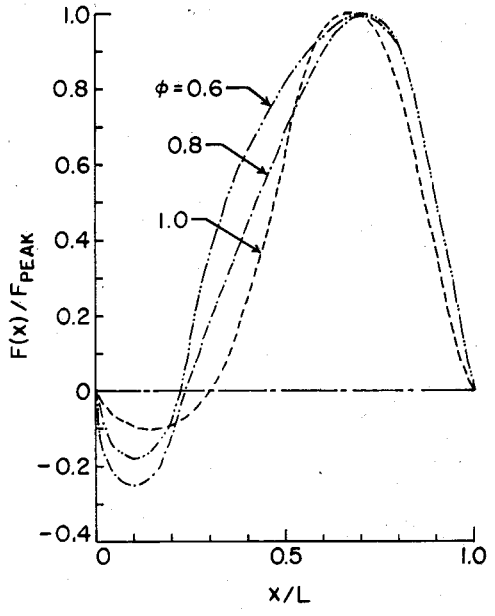

Fig. 10 $F(x)$ vs length along flame axis for various flames at a frequency of 300 Hz.

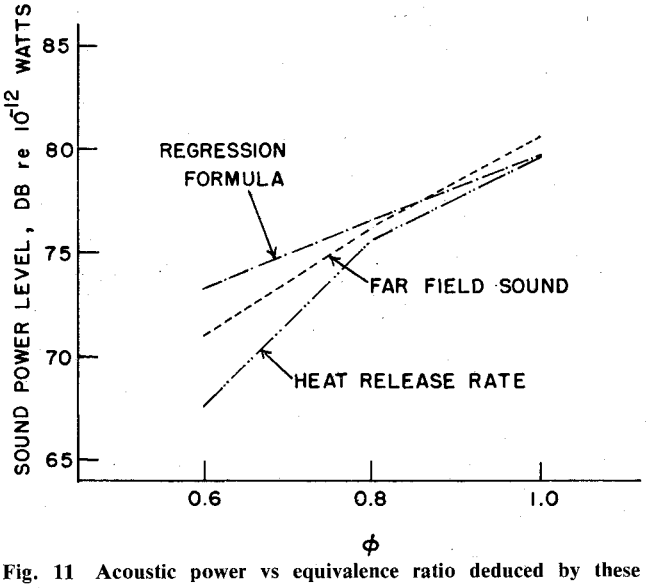

Fig. 11 Acoustic power vs equivalence ratio deduced by these methods.

shape. The implication is that the shape of the mean heat release rate distribution can be deduced from the fluctuating heat release rate obtained by the acoustic technique.

Correlation Experiments

Figure 9 shows the coherence function between p and the time derivative of the light emission intensity for various ϕ. The high value of the coherence function for $\phi = 1.0$ and 0.8 up to 500 Hz implies an almost linear relationship between the

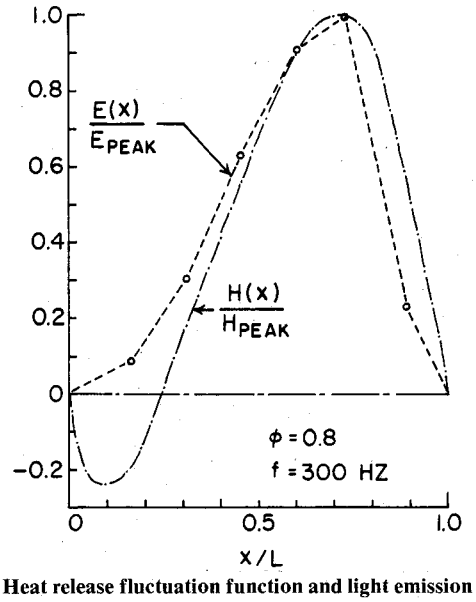

Fig. 12 Heat release fluctuation function and light emission function vs length along flame axis for the $\phi = 0.8$ flame at 300 Hz.

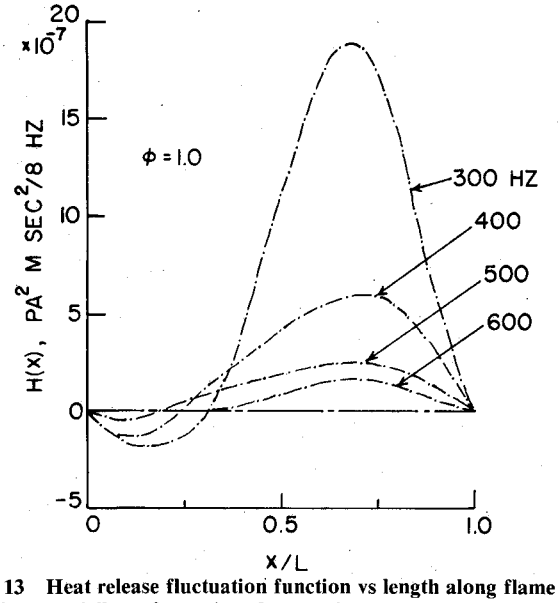

Fig. 13 Heat release fluctuation function vs length along flame axis for the $\phi = 1.0$ flame for various frequencies.

sound and light emissions. The drop in the coherence function at high frequencies may be due to the noise introduced by differentiation of the light signal in the time domain. The coherence is poor for $\phi = 0.6$. A distinguishing feature of this flame is that it is about twice as long as the other two flames. There is more scope in the longer flame for the air entrainment causing dilution of the reaction zone. This would affect the concentration of radicals and may explain the low coherence.

VI. Computed Results

Having obtained the sound data by experiment, the next step is to solve Eq. (7) for $F(x)$. As mentioned earlier, the solution of a first-kind integral equation is a formidable problem, especially when the input data contain errors. Equation (7) is the result of various simplifications, based on physical grounds, made to the original six-dimensional equation. Still, any further knowledge of the behavior of the expected solution would be helpful. Here it is intuitively obvious that $F(x)$ has to be zero at the flame ends. These conditions were incorporated into the solution procedure.

The computational work was carried out on a CDC CYBER 70 Model 74-28 computer. A Fourier series was chosen for $F(x)$,

$$F(x) = a_0 + \sum_n \left(a_n \cos \frac{2n\pi x}{L} + b_n \sin \frac{2n\pi x}{L} \right), \quad 0 \le x \le L$$

The Galerkin matrices were evaluated by a 15 point Gauss Chebyshev quadrature. Linear programming was done using the IMSL subroutine[15] ZX4LP, which is based on the revised simplex algorithm.

Figure 10 shows the results for the three flames for a particular frequency. They were obtained with a seven-term Fourier expansion for $y_R = 127$ mm, $\lambda = 3$, $r = 4$. $F(x)$ is seen to be negative near $x = 0$. Actually, the heat release autospectrum cannot be negative. However, the negative portion is quite small compared to the large peak in the second half of the flame and may be ignored. The peaks lie in the region $x/L = 0.5$-0.75.

Comparison of Overall Acoustic Power

A verification of the computed results is obtained by calculating the overall acoustic power from $F(x)$ and comparing it with the value obtained directly. Since combustion noise radiation is known to be only weakly directional, a good approximation to the overall acoustic power is obtained from a single microphone measurement in the far field. Also, a regression formula[10] is available, which gives acoustic power for hydrocarbon-air open turbulent flames in terms of burner diameter, flow speed, and mixture composition. The sound power levels computed by the three methods are plotted against equivalence ratio in Fig. 11. There is good qualitative agreement between all the three methods.

Comparison with Optical Emission Experiments

The optical experiments were conducted to provide qualitative verification of the results computed by the acoustic technique. In these experiments, cross-spectral densities of C_2 emission intensity were determined for several flame cross sections. From these data, length scales were calculated. In order to compare the acoustic and optical results, two new functions are defined here. The first is the heat release fluctuation function $H(x)$,

$$H(x) = F(x)/f^2$$

From Sec. II, $F(x) \propto f^2 S_{\hat{Q}\hat{Q}} L_{\hat{Q}}$. Hence,

$$H(x) \propto \left[\begin{array}{l} \text{Heat release rate} \\ \text{autospectral density} \end{array} \right] \text{(length scale)}$$

The second function is the light emission fluctuation function $E(x)$ defined by

$$E(x) = S_{II}(L_{\hat{Q}}/D)$$

where S_{II} is the C_2 emission autospectral density. Since C_2 emission is proportional to heat release rate,

$$E(x) \propto \left[\begin{array}{l} \text{Heat release rate} \\ \text{autospectral density} \end{array} \right] \text{(length scale)}$$

In other words, the functions $H(x)$ and $E(x)$ measure the same quantity to within a factor of a constant. They are shown in Fig. 12 for $\phi = 0.8$, $f = 300$ Hz. There is good qualitative agreement between the two curves. Both are small near the burner port. Also, both peak near three-fourths of the flame length and drop sharply toward the tip of the flame. Considering the various approximations involved in arriving at Eq. (7) and the solution $F(x)$ the similarity in shape is striking. The functions $H(x)$ and $E(x)$ are plotted in Figs. 13 and 14, respectively, for the $\phi = 1.0$ flame with frequency as a parameter. Again, there is matching of the shapes. Both functions drop as frequency increases.

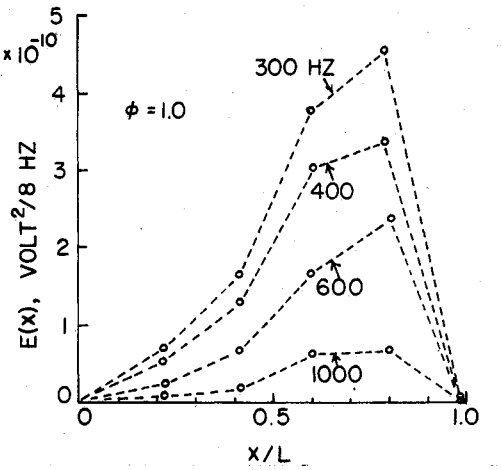

Fig. 14 Light emission function vs length along flame axis for the $\phi = 1.0$ flame for various frequencies.

VII. Conclusions and Recommendations

A nonintrusive acoustic technique has been developed to obtain the fluctuating heat release rate distribution in open premixed turbulent flames. Propane-air flames of equivalence ratios 0.6, 0.8, and 1.0 have been employed. The burner size was 16.4 mm and the mean flow speed was 11.55 m/s. The heat release rate fluctuations are related to combustion noise spectra by a Fredholm integral equation of the first kind. This type of equation is known to be unstable inasmuch as the solution tends to be highly sensitive to errors in the input data. Sound pressures in the near field of the flames were measured in an anechoic chamber and the equation was solved by an augmented Galerkin method. The technique is shown to be stable to perturbations in the data.

For the $\phi = 0.8$ and 1.0 flames, good coherence is shown to exist between the far-field acoustic pressure and the time derivative of the emission intensity of C_2 radicals in the flame. For these flames the results computed from the near-field pressure measurements have been verified qualitatively by the C_2 emission studies, thus providing independent experimental support.

From the optical experiments, the cross-sectional heat release rate fluctuations were found to have an integral length scale of the order of the burner diameter. The autospectral density of these fluctuations multiplied by the length scale showed a single peak near the flame tip.

It is observed that there is similarity in shape between plots of mean and rms values of C_2 emission intensity along the flame axis. The implication is that the shape of the mean heat release rate distribution can, in principle, be deduced by the acoustic technique.

It is suggested that the technique be extended to a gas turbine combustor. Because of the instability problems associated with the integral equation formulation, it would be preferable to solve the appropriate differential equations. Nonintrusive acoustic measurements could be made by pressure transducers mounted in the combustion chamber wall.

Acknowledgments

This work was supported by the U.S. Army Research Office under Contract DAAG 29-79-C-0087. The authors appreciate the assistance of Dr. G. K. Mehta during the conduct of the experiments.

References

[1]Strahle, W. C., "On Combustion Generated Noise," *Journal of Fluid Mechanics*, Vol. 49, Pt. 2, 1971, pp. 399-414.

[2]Strahle, W. C., "Some Results in Combustion Generated Noise," *Journal of Sound and Vibration*, Vol. 23, 1971, pp. 113-125.

[3]Strahle, W. C., "Combustion Noise," *Progress in Energy and Combustion Science*, Vol. 4, 1978, pp. 157-176.

[4]Morse, P. M. and Ingard, K. U., *Theoretical Acoustics*, 1st ed., McGraw Hill Book Co., New York, 1968, p. 321.

[5]Bendat, J. S. and Piersol, A. G., *Random Data: Analysis and Measurement Procedures*, 1st ed., Wiley-Interscience, New York, 1971, Chap. 1.

[6]Baker, C.T.H., *The Numerical Treatment of Integral Equations*, Clarendon Press, Oxford, England, 1977.

[7]Miller, G. F., "Fredholm Equations of First Kind," *Numerical Solution of Integral Equations*, edited by L. M. Delves and J. Walsh, Clarendon Press, Oxford, England, 1974, pp. 175-188.

[8]Babolian, E. and Delves, L. M., "An Augmented Galerkin Method for First Kind Fredholm Equations," *Institute of Mathematics and Its Applications Journal*, Vol. 24, 1979, pp. 157-174.

[9]Ramachandra, M. K., "A Study of Heat Release Rate Distribution in Open Premixed Turbulent Flames by Acoustic Measurements," Ph.D. Thesis, Georgia Institute of Technology, Atlanta, Ga., 1981, Chap. III.

[10]Shivashankara, B. N., "An Experimental Study of Noise Produced by Open Turbulent Flames," Ph.D. Thesis, Georgia Institute of Technology, Atlanta, Ga., 1973, Chaps. II and IV.

[11]Hurle, I. R., Price, R. B., Sugden, T. M., and Thomas, A., "Sound Emission from Open Turbulent Premixed Flames," *Proceedings of the Royal Society of London*, Vol. A303, 1968, pp. 409-427.

[12]Price, R. B., Hurle, I. R., and Sugden, T. M., "Optical Studies of the Generation of Noise in Turbulent Flames," *Twelfth Symposium (International) on Combustion*, The Combustion Institute, Pittsburgh, Pa., 1969, pp. 1093-1102.

[13]Wortberg, G., "Ion-Concentration Measurements in a Flat Flame at Atmospheric Pressure," *Tenth Symposium (International) on Combustion*, The Combustion Institute, Pittsburgh, Pa., 1965, pp. 651-655.

[14]Mehta, G. K., Ramachandra, M. K., and Strahle, W. C., "Correlations between Light Emission, Acoustic Emission and Ion Density in Premixed Turbulent Flames," *Eighteenth Symposium (International) on Combustion*, The Combustion Institute, Pittsburgh, Pa., 1981, pp. 1051-1059.

[15]*International Mathematical and Statistical Library*, 8th ed., IMSL Inc., Houston, Tex., 1980, Vol. 3.